energy&fuels

pubs.acs.org/EF Article

One-Step Hydropyrolysis and Hydrotreating Tandem Reactions of *Miscanthus* × *giganteus* Using Ni Impregnated ZSM-5/MCM-41 Composites

Lei Yu,[§] Azeem Farinmade,[§] Oluwole Ajumobi, Vijay T. John,* and Julia A. Valla*

Cite This: *Energy Fuels* 2021, 35, 20117−20130 Read Online

ACCESS | Metrics & More | Article Recommendations | Supporting Information

ABSTRACT: In this study, we propose that the multistep, tandem catalytic fast hydropyrolysis (CFHP) and hydrotreatment reactions of biomass to produce gasoline and diesel grade biofuels can be conducted in a single step process using a composite of Ni-ZSM-5 microcrystals encapsulated in spherical particles of Ni-MCM-41 (Ni-ZSM-5/Ni-MCM-41). The composite has been successfully prepared *via* a one-step aerosol method and characterized by N_2 adsorption−desorption, X-ray diffraction, scanning electron microscope (SEM), transmission electron microscope (TEM), pyridine adsorption, inductively coupled plasma-optical emission spectrometry (ICP-OES), and H_2 chemisorption. The composite has been tested for one-stage CFHP and hydrotreatment of *Miscanthus* × *giganteus* at 600 and 500 °C. The product yields and distribution derived from the one-stage CFHP and hydrotreatment of *Miscanthus* × *giganteus* using the Ni-ZSM-5/Ni-MCM-41 composite were compared to those of a typical two-stage process, with Ni-ZSM-5 in the first stage (CFHP) and Ni-MCM-41 in the second stage (hydrotreatment). Additional experiments were carried out using Ni-ZSM-5, Ni-ZSM-5/MCM-41, and ZSM-5/Ni-MCM-41 composites, as well as physical mixtures of Ni-ZSM-5 and Ni-MCM-41 to obtain further insights into the role of each part of the composites to the product yields and distribution derived from the one-stage CFHP and hydrotreatment reaction. The comparison of results showed that the Ni-ZSM-5/Ni-MCM-41 composite enhanced the production of alkanes and methane without sacrificing the yield to monoaromatic hydrocarbons. Therefore, this study proves that such a unique composite can complete the two-step tandem reactions in one single step, leading to a self-sustainable and intensified process.

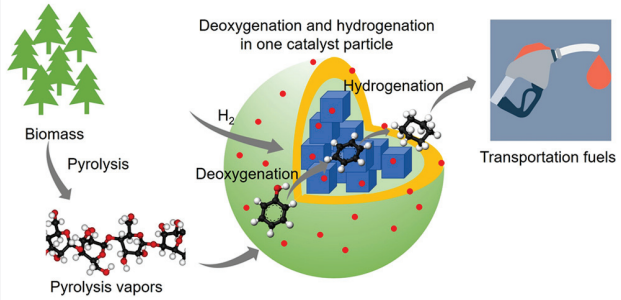

1. INTRODUCTION

The massive energy needs of our modern society and the depletion of fossil fuels are calling for renewable energy resources.[1−3] Biomass is a widely available resource that is considered as one of the few possible resources of renewable carbon and can be used for clean liquid fuels production, such as biogasoline and biodiesel.[4−6] The thermochemical technologies of biomass conversion, including torrefaction, liquefaction, pyrolysis, and gasification,[7] have drawn great attention in recent years.[8] Biomass pyrolysis operates at inert atmosphere and high temperature and leads to the production of liquid fuels (bio-oil) and two byproducts, namely, biochar and noncondensable gases.[9] Nevertheless, the raw bio-oil derived from the direct pyrolysis of biomass contains water and oxygenates; thus, it is acidic, viscous, and unstable and has a low calorific value.[10−12] Therefore, the bio-oil cannot be used directly after pyrolysis. Instead, an upgrading step with the assistance of catalysts *in situ* or *ex situ* the pyrolysis process is necessary.[13] Catalytic fast pyrolysis (CFP) is a typical process that produces high quality bio-oil directly from biomass.[14−17] However, low bio-oil yields and rapid coke formation have been major challenges toward the commercialization of CFP.[18−20]

Catalytic fast hydropyrolysis (CFHP) has shown substantial advantages compared to CFP.[21] Hydropyrolysis involves the presence of hydrogen, which differs from the inert atmosphere of pyrolysis.[22] CFHP leads to more deoxygenated fuels and less coke compared to CFP.[23,24] CFHP is an exothermic reaction, which is one of the most important advantages of CFHP compared to CFP, which is endothermic.[23,25,26] Another crucial advantage of CFHP over CFP is that the former removes oxygen more likely *via* dehydration reactions followed by hydrogenation and hydrodeoxygenation reactions rather than decarboxylation or decarbonylation reactions, thus minimizing the carbon loss during the process.[5,24,27] The

Received: July 20, 2021
Revised: October 28, 2021
Published: November 12, 2021

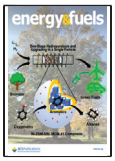

https://doi.org/10.1021/acs.energyfuels.1c02453
Energy Fuels 2021, 35, 20117−20130

concept of hydropyrolysis was first proposed for the conversion of coal[28] and later applied for biomass.[4] CFHP of biomass did not receive considerable attention until approximately 10 years ago.[29] The fast hydropyrolysis of biomass involves four possible configurations: noncatalytic fast hydropyrolysis (one-step), *in situ* CFHP (one-step), noncatalytic fast hydropyrolysis with *ex situ* hydrotreating (two-step), and *in situ* CFHP with *ex situ* hydrotreating (two-step).[4] Noncatalytic fast hydropyrolysis does not involve the use of catalysts and simply substitutes inert gas (pyrolysis) with hydrogen (hydropyrolysis). The use of hydrogen without a catalyst does not affect the solid yield and liquid product distribution significantly, although a slight increase in hydrocarbon yield has been observed.[27,30,31] The *in situ* CFHP involves the use of catalysts, such as ZSM-5,[32] Ni-ZSM-5,[33] Pd-ZSM-5,[34] and MCM-41,[27] in the pyrolysis step. Compared to *in situ* CFP, it leads to a lower coke and higher liquid yield, with higher selectivity to hydrocarbons.[35,36] The noncatalytic fast hydropyrolysis with *ex situ* hydrotreating can be regarded as *in situ* hydrodeoxygenation (HDO), where the raw bio-oil is upgraded after it is vaporized. Vapor phase catalytic upgrading right after hydropyrolysis is beneficial over traditional HDO, because it can avoid secondary reactions during condensation and revaporization of the pyrolyzate.[5,31] Compared to *in situ* CFHP, the two-step noncatalytic hydropyrolysis followed by *ex situ* hydrotreatment allows for independent control of hydropyrolysis and catalytic upgrading at their respective optimal conditions.[37,38] The two-step *in situ* CFHP followed by *ex situ* hydrotreatment is a combination of the second and third configurations and allows for independent control of the two steps and complete deoxygenation and hydrogenation of the bio-oil compounds, thus producing gasoline and diesel range fuels.[39,40]

According to the modified Van Krevelen diagram,[41] even the most deoxygenated bio-oil derived from CFP has an atomic H/C ratio of about 1, which is close to the range of coal, while the typical H/C ratios of gasoline and diesel are close to 2. Hence, the deoxygenated bio-oils still require some level of hydrotreatment to obtain a high fuel quality, ready for transportation use. In this circumstance, the CFHP with *ex situ* hydrotreating can be a promising configuration. Obviously, the disadvantage of such configuration is that multiple reactors and catalytic steps are involved, which results in a higher cost and energy consumption. Only a few studies have reported the use of the aforementioned two-stage CFHP and hydrotreatment configuration. To the best of our knowledge, researchers from Gas Technology Institute (GTI) were the first to report this setup.[39,40] The process is called IH^2, where the hydropyrolysis, hydroconversion, and steam reforming are integrated in one system and a continuous production of gasoline and diesel range fuels from biomass is accomplished. Besides the above, Sirous-Rezaei et al. reported the use of HY as an active *in situ* hydropyrolysis catalyst followed by an *ex situ* upgrading using various catalysts (Fe/HBeta, $FeReO_x$/MCM-41, Fe/ZrO_2, and $FeReO_x$/ZrO_2).[42] Although a greater aromatic hydrocarbon yield was observed with the secondary upgrading reactor, no saturated cyclic compounds were detected in the liquid products. In our previously published work,[41] we have demonstrated that the upgrading of bio-oil derived from *in situ* CFHP in a second stage hydrotreatment process could result in a shift of liquid carbon yields from monocyclic aromatics and naphthalenes to alkanes, so that drop-in biofuel can be produced directly from a two-stage CFHP followed by an upgrading process.

Nevertheless, the major challenge of a successful CFHP with or without a downstream upgrading step is the production of gasoline and diesel range biofuels with a high alkanes content. The one-step CFHP results by Jan et al. showed that a lower pyrolysis temperature is favorable for alkane production, although the total hydrocarbon yield might be suppressed.[34] In addition, the use of metals, such as Ni[24,35,43] and Pd,[34] on various supports is beneficial for a higher alkane yield. Our previous study proved that Ni-SiO_2 could enhance the production of alkanes with the sacrifice of other hydrocarbon yields compared to Ni-ZSM-5 during the *in situ* CFHP.[44] Stummann et al. evaluated various catalysts in a fluid bed hydropyrolysis reactor with or without additional HDO in a second stage.[45] They observed that the second stage HDO significantly improved the selectivity to hydrocarbons, especially to naphthenes (cycloalkanes). Another study also conducted by Stummann et al. explored the effects of temperature and pressure on product distributions.[46] They found that a higher pressure and lower fluid bed temperature (below 405 °C) promoted the production of cycloalkanes, while the aromatic yields were sacrificed. Dayton et al. investigated the effect of various operating conditions on the product distribution of *in situ* CFHP in a fluidized bed reactor.[47] They demonstrated that the increase of H_2 partial pressure or the increase of reactor temperature would enhance the production of aliphatics. Venkatesan et al. observed high alkane yield at a H_2 partial pressure of 20 bar and a catalyst bed temperature of 350 °C,[5] indicating that a relatively low temperature is more suitable for second-stage hydrotreatment, as it is an exothermic reaction. Venkatesan et al.[48] tested γ-Al_2O_3 for two-stage noncatalytic hydropyrolysis with second stage upgrading of pine-wood, and it showed good selectivity to alkanes.

Summarizing, it has been demonstrated that *in situ* CFHP coupled with second-stage hydrotreatment can be beneficial for the production of higher quality biofuels. However, the cost and energy consumption associated with the two-stage process in addition to the low selectivity to alkanes can be major challenges. In our previous work,[19,49] we have demonstrated that MCM-41/ZSM-5 composites with various ZSM-5 concentrations can substantially enhance CFP reactions and reduce the rate of coke formation on catalysts. Specifically, we have demonstrated that ZSM-5 can be successfully encapsulated into MCM-41 particles; during CFP, the vapors can diffuse through the MCM-41 pores, contact the ZSM-5 active sites, react (through cracking and deoxygenation), and diffuse out of the MCM-41 as smaller hydrocarbon molecules. In this multistep reaction process, MCM-41 acts as a sacrificial layer for initial cracking reactions and coke deposition, allowing the ZSM-5 sites to be active for a longer time. Driven by these promising results, here, we propose that the composite can be an outstanding candidate for tandem catalytic reactions, such as the two-stage CFHP followed by hydrotreatment. Thus, our hypothesis is that metal impregnated ZSM-5/MCM-41 composites can realize the *in situ* CFHP and *ex situ* hydrotreating upgrading process in just a single catalytic step, where the pyrolysis vapors can be first hydrocracked to small molecules on Ni-MCM-41 surface and then deoxygenated within the encapsulated Ni-ZSM-5 and the products can be subsequently hydrotreated as they diffuse out of the Ni-MCM-41 surface. Thus, the secondary reactor for hydrotreat-

https://doi.org/10.1021/acs.energyfuels.1c02453
Energy Fuels 2021, 35, 20117−20130

ment can be eliminated and the hydrotreating reactions can be completed simultaneously with the primary CFHP process, increasing the selectivity toward alkanes and resulting in a significant process intensification. The objective of this study was to explore whether such a Ni-ZSM-5/Ni-MCM-41 composite can bring the tandem CFHP and hydrotreating reactions together in one catalyst particle. Such catalyst can have substantial industrial significance, especially in the biomass petrochemical, and hydrocarbon production and processing areas.

2. MATERIALS AND METHODS

2.1. Materials. The biomass used in this study was *Miscanthus* × *giganteus*. The detailed compositions (ultimate and proximate analysis) of the biomass can be found in our previous studies[17,50] or in the Supporting Information (SI). Hexadecyltrimethylammonium bromide (CTAB, 95%), nickel(II) nitrate hexahydrate ($Ni(NO_3)_2 \cdot 6H_2O$), and tetraethyl orthosilicate (TEOS, 98%) were purchased from Sigma-Aldrich and were used without any modifications. Nanosized ZSM-5 (300 nm of crystal size, with a SiO_2/Al_2O_3 molar ratio of 26) was purchased from ACS Material. MCM-41 and ZSM-5/MCM-41 composites were prepared in the lab using the aerosol method following the protocol that was published previously.[49] A schematic of the aerosol method can be found in Figure S1. Briefly, for the synthesis of spherical MCM-41 particles, 1.5 g of CTAB and 2 mL of 0.1 M HCl were added to 15 mL of ethanol in a vial, followed by the dropwise addition of 4.5 mL of TEOS under magnetic stirring. The silica precursor solution was left to stir at room temperature for 10 min before being transferred into a nebulizer. The aerosolization of the silica precursor solution by N_2 gas (2.5 L/min) led to the formation of fine droplet mists that were carried into the tubular furnace. In the furnace heating zone operating at 400 °C, rapid hydrolysis and condensation reaction occurred in each droplet, leading to the formation of solid silica particles. The silica particles were collected over a filter at the end of the tubular furnace. Postsynthesis removal of surfactant template was carried out by calcination in air at 550 °C for 8 h. The synthesis of the ZSM-5/MCM-41 or Ni-ZSM-5/MCM-41 composites follows the same methods for MCM-41 except that 0.56 g of ZSM-5 or Ni-ZSM-5 was dispersed into the silica precursor solution prior to transferring it to the nebulizer for aerosolization.

Various composites were prepared with a constant concentration of ZSM-5 (50% on silica molar ratio basis or 32% on mass basis) and different metal locations. The incorporation of metal follows a standard incipient wetness impregnation method[51] using $Ni(NO_3)_2 \cdot 6H_2O$ for the metal loading of Ni. The impregnated samples were then calcined at 550 °C in air for 4 h and reduced at 550 °C in H_2 for 4 h. On the basis of the location of metal, the composites were named as Ni-ZSM-5/MCM-41 (5 wt % of Ni impregnated in ZSM-5 and encapsulated in MCM-41), ZSM-5/Ni-MCM-41 (ZSM-5 encapsulated in MCM-41 and then impregnated with 5 wt % of Ni on the basis of the mass of MCM-41), and Ni-ZSM-5/Ni-MCM-41 (5 wt % of Ni impregnated in ZSM-5, encapsulated in MCM-41 and then impregnated with 5 wt % of Ni on the basis of the mass of MCM-41). Scheme 1 illustrates the structures and Ni locations of Ni-ZSM-5 and composites. In addition to the composites, a physical mixture of 5 wt % Ni on ZSM-5 (Ni-ZSM-5) and 5 wt % Ni on MCM-41 (Ni-MCM-41) was also prepared following the same mass ratio of Ni-ZSM-5 and Ni-MCM-41 in the composite Ni-ZSM-5/Ni-MCM-41.

2.2. Materials Characterization. The prepared catalysts were characterized by N_2 adsorption−desorption using a Micromeritics ASAP 2020 Physisorption Analyzer. Prior to analysis, each sample was degassed for 12 h at 120 °C under high vacuum. N_2 adsorption−desorption isotherms were collected at 77 K after degassing. Surface areas were calculated on the basis of Brunauer−Emmett−Teller (BET) method. The BET plot was fitted with a range of P/P_0 between 0.05 and 0.2 with eight data points. Pore size distribution was determined using the Barrett−Joyner−Halenda (BJH) method. The

Scheme 1. Representations of Ni-ZSM-5 and the Composites: (a) Ni-ZSM-5, (b) Ni-ZSM-5/MCM-41, (c) ZSM-5/Ni-MCM-41, and (d) Ni-ZSM-5/Ni-MCM-41

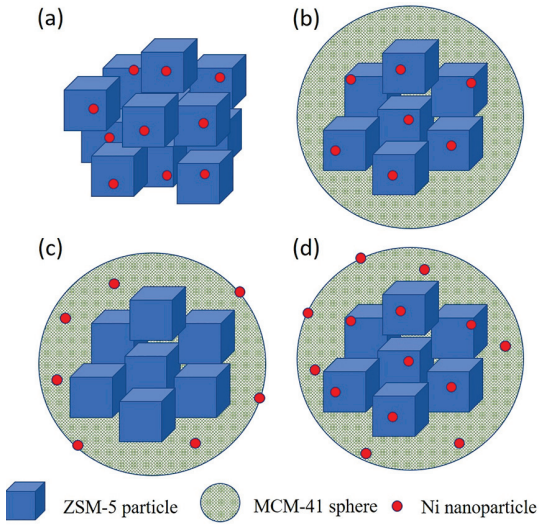

total pore volume was obtained from single point adsorption below $P/P_0 = 0.99$. The micropore volume was derived from a t-plot.

X-ray diffraction (XRD) analysis of all catalysts was performed on a Rigaku Miniflex II using Cu Kα radiation at 1.54 Å. For each analysis, the sampling width was set to 0.1° while the scan was conducted in continuous mode at 2°/min. The small angle XRD scan was performed from 2θ = 1.5° to 6° using a 0.625° divergent slit, and the wide-angle diffraction scan was from 2θ = 6° to 60° using a 1.25° divergent slit.

Electron microscopy was performed to visualize the morphology of the catalyst. Scanning electron microscopy (SEM) was performed using a Hitachi S-4800 field emission scanning electron microscope operated at 3 kV. The catalyst samples were prepared for SEM imaging by dispersing in anhydrous ethanol. An aliquot of the dispersed sample was then placed on an aluminum stub and the solvent was evaporated. The sample was carbon coated by sputtering a thin coating of carbon from a graphite source to improve the sample conductivity for imaging. Transmission electron microscopy (TEM) was performed using an FEI Tecnai G2 F30 twin transmission electron microscope operated at 300 kV. An aliquot of the dilute catalyst samples dispersed in anhydrous ethanol was dropped onto a copper TEM grid (PELCO Grids, 200 mesh, 3.0 mm O.D.). The ethanol solvent was evaporated completely at room temperature before the TEM grid was mounted onto the sample grid holder for loading into the TEM vacuum chamber. Ni particle size distribution was estimated by the TEM images, and the results are shown in Figure S3.

The Brønsted acid and Lewis acid site concentrations of catalysts were determined *via* pyridine adsorption in a diffuse reflectance infrared fourier transform spectroscopy (DRIFTS) unit. The instrument is composed of a Thermo Nicolet 6700 FTIR spectrometer coupled with a temperature-controlled Harrick Praying Mantis DRIFTS accessory. The background was collected using KBr at 120 °C under a N_2 atmosphere. Prior to pyridine adsorption, the spectra of catalysts were collected at 120 °C with a N_2 purge. The pyridine was then flowed into the DRIFTS cell carried by N_2 flow for 20 min until the catalysts were saturated by pyridine. After adsorption, the cell was heated to 240 °C under a vacuum and held for 30 min to remove physisorbed pyridine. The cell was then cooled to 120 °C to take the spectra. The final spectra were derived by subtracting the spectra before adsorption from the spectra after adsorption. Therefore, the peaks shown in the spectra are only attributed to the chemisorption of pyridine. The results are shown in the SI.

https://doi.org/10.1021/acs.energyfuels.1c02453
Energy Fuels 2021, 35, 20117−20130

Scheme 2. Configuration of Py-GC/MS System for the CFHP of Biomass

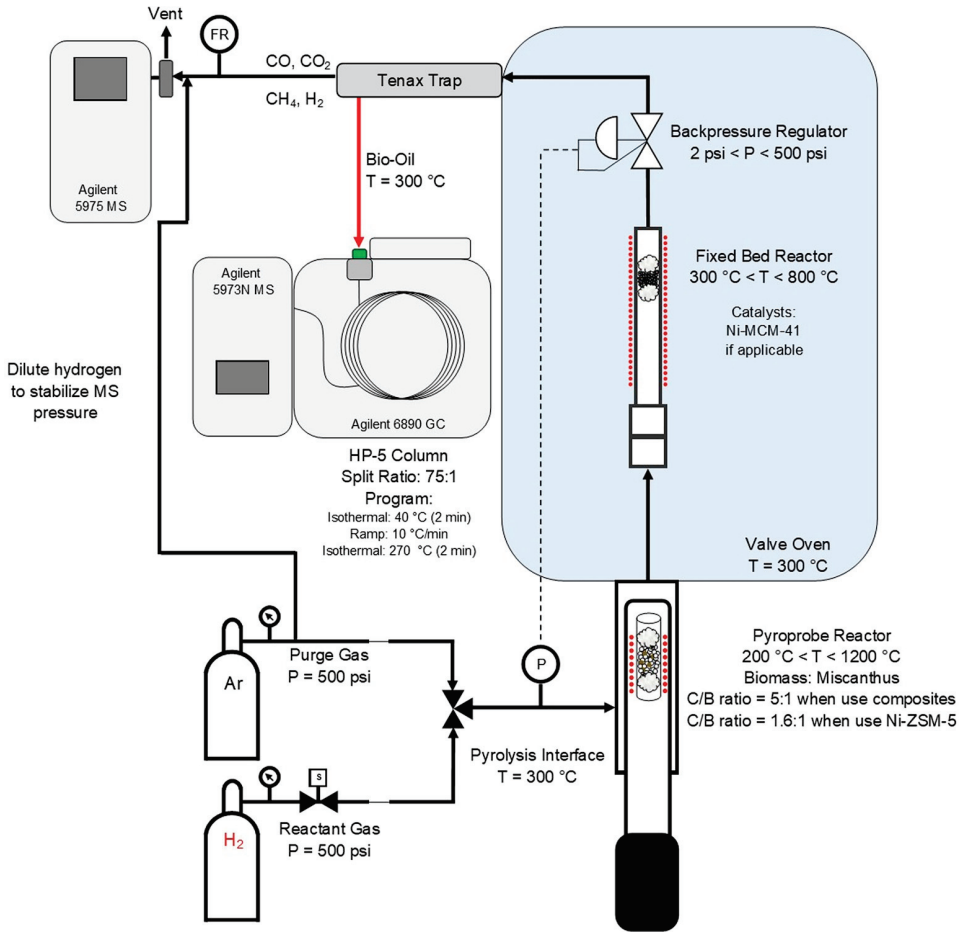

The actual Ni loading on catalysts was measured by inductively coupled plasma optical emission spectroscopy (ICP-OES). The analysis was performed using a PerkinElmer 7300DV Dual View inductively coupled plasma optical emission spectrometer according to established protocols. In summary, approximately 0.01−0.038 g of the sample as removed, homogenized, and placed into a hot block tube. Trace metal grade hydrochloric (0.75 mL) and nitric (2.25 mL) acids were added to each tube and placed in the hot block and refluxed for 3 h at 95 °C. The samples were cooled and brought up the final volume of 25 mL with DI water. All samples were analyzed at 50× dilution due to the very high levels of the target elements in the samples. Standard quality assurance procedures were employed, including an analysis of initial and continuing calibration checks and blanks, duplicate samples, preparation blanks (Blank), postdigestion spiked samples, and laboratory control samples (LCS).

The metal dispersion was measured by H_2 chemisorption using a Micromeritics ASAP 2020C Chemisorption Analyzer. The samples were degassed and reduced *in situ* and analyzed at 35 °C.

2.3. CFHP and Hydrotreatment Experiments. All experiments were carried out in a pyrolysis gas chromatography/mass spectrometer (Py-GC/MS) system (CDS Analytical 5200HP). Scheme 2 shows a schematic of the Py-GC/MS system used in this study. The system includes two reactors: the pyroprobe reactor, where the pyrolysis occurs, and the fixed-bed reactor, where the second-stage hydrotreatment takes place. In this study, Ar (UHP 300, Airgas) was used as the purge gas and H_2 (UHP 80, Airgas) was used as carrier gas during the experiments. The pressure of the reactors was maintained by a back-pressure regulator, which was adjusted to the desired operating pressure prior to experiments. The gas flow rate was measured by a flowmeter placed at the outlet of the unit. The pyrolyzer heating rate was set as 999 °C/s. All lines and the valve oven were maintained at 300 °C to avoid any condensation of pyrolyzate vapors. The condensable vapors were trapped in a cold adsorption column (Tenax, Dow Chemical), and the permanent gas traveled through the unit and was finally analyzed by a real-time mass spectrometer (MS). The trapped volatiles were revaporized at 300 °C after the permanent gas passed through the column. Ar was also flowed through an external gas line (300 mL/min) and merged with H_2 and gas products coming from the outlet of the system before entering MS. This kept the pressure of MS stable and allowed for more accurate measurement of gas signals. Note that in this study we used a Py-GC/MS system, which is a reactor setup very different from the fixed or fluidized bed reactors. Thus, care should be taken in making direct comparison of results obtained in this study to those obtained using other reactor designs.[5,23,36,45,46] However, in our previous published study,[17] we demonstrated that the Py-GC/MS reactor can be a powerful tool to evaluate various catalysts and operating conditions of biomass pyrolysis and the trends of the results are consistent with a spouted bed reactor. Thus, we believe that the results of this study can provide important information and guidance for further studies using more conventional reactors.

Four experimental scenarios were explored in this study: Scenario 1, one-stage CFHP using Ni-ZSM-5 catalyst (control experiment); Scenario 2, CFHP and hydrotreatment in one-stage using the composites Ni-ZSM-5/MCM-41, ZSM-5/Ni-MCM-41, and Ni-ZSM-5/Ni-MCM-41; Scenario 3, one-stage CFHP and hydrotreatment using the physical mixture of Ni-ZSM-5 and Ni-MCM-41; Scenario 4. CFHP followed by hydrotreatment in two-stages using Ni-ZSM-5 and Ni-MCM-41, respectively. Scenario 1 was performed for comparison reasons and to better understand the role and the importance of the

https://doi.org/10.1021/acs.energyfuels.1c02453
Energy Fuels 2021, 35, 20117−20130

Scheme 3. Simplified Schematic of the Four Experimental Scenarios

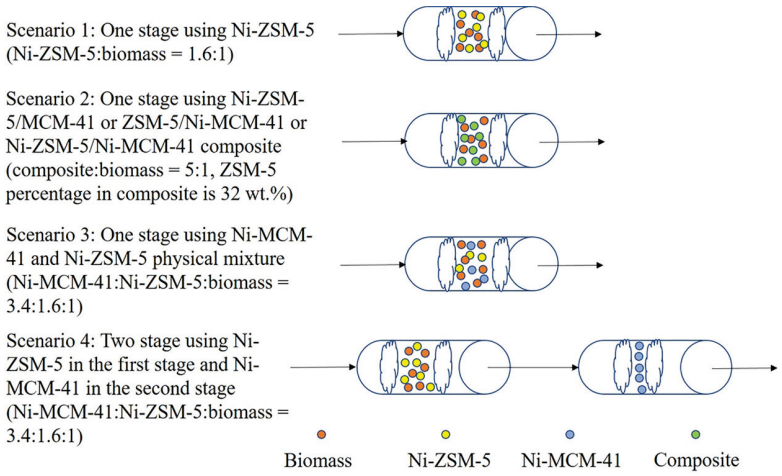

hydrotreatment step performed in the other Scenarios. Scenario 2 was performed to understand the feasibility of one-stage CFHP and hydrotreatment reactions using the composites and to investigate the impact of Ni location in the composite on the product distribution. The objective of Scenario 3 was to understand the role of composite structure compared to the simple physical mixture of Ni-MCM-41 and Ni-ZSM-5. Finally, the objective of Scenario 4 was to prove the hypothesis that the composites can effectively complete the two-stage CFHP and hydrotreatment reactions in one-stage, by comparing the results with Scenario 2. Scheme 3 demonstrates the four different scenarios. The detailed mass of biomass and catalyst used in each scenario are summarized in Table S2.

All the experiments were performed at pyrolysis (the first stage) temperatures of 500 and 600 °C. For Scenario 4, the second hydrotreatment stage was maintained at 300 °C, since relatively low temperatures favor the hydrotreatment reactions, as discussed in the Introduction section. Prior to the experiments, catalysts and biomass were well-mixed. For Scenario 2, the composites were mixed with biomass at a catalyst/biomass (C/B) ratio of 5:1. For Scenarios 1 and 4, where Ni-ZSM-5 and biomass were mixed in the first stage, the Ni-ZSM-5 to biomass ratio was maintained at 1.6:1, since we have shown in our previous study that the MCM-41 layer is basically inert to the reaction.[19] Thus, basically the Ni-ZSM-5 to biomass ratio was the same in all Scenarios. Additionally, in Scenario 4, Ni-MCM-41 was placed separately in the second stage with a mass ratio to the biomass of 3.4:1, which was equal to the mass ratio of Ni-MCM-41 to biomass in Scenario 2 (composites). Finally, in Scenario 3, the mass ratio of Ni-MCM-41/Ni-ZSM-5/biomass was 3.4:1.6:1 to match the mass ratio of each components in Scenario 2. For a typical run, 5 ± 0.1 mg of the mixture (catalyst and biomass) was loaded into a micro quartz tube and sandwiched by two pieces of quartz wool. The microreactor was then placed in the platinum pyrolysis probe that would be inserted into the pyrolysis interface. In the case of two-stage experiments, 6.5 ± 0.1 mg of Ni-MCM-41 was added to the fixed-bed reactor (the second stage) and held by two pieces of quartz wool. After the system was leak checked and purged with Ar, hydrogen was fed to the system at a flow rate of 110 mL/min *via* the reactive gas port. The system was purged by hydrogen for 5 min prior to pyrolysis, allowing the system to be stabilized. All the CFHP experiments were conducted at a pressure of 31 bar with a pyrolysis duration of 20 s. The experiments were repeated three times to ensure the reproducibility of the experiments.

For all the CFHP experiments, the condensable liquid products were analyzed by gas chromatography−mass spectrometry (GC−MS, Agilent 6890 GC coupled with HP-5 column and 5973 N MS). When the pyrolysis was completed and the system was purged, the volatiles adsorbed on the cold trap were desorbed and sent to the GC−MS through a heated line for composition analysis. The oven temperature was initially maintained at 40 °C for 2 min, then ramped up with a heating rate of 10 °C/min to 270 °C, followed by another 2 min isothermal step. The GC−MS was calibrated externally by injecting prepared standard mixture from the pyrolyzer. The directly calibrated compounds were benzene, toluene, xylene, phenol, benzofuran, naphthalene, and phenanthrene. The semiquantification was applied to the products that were not directly calibrated, on the basis of their molecular weight and functional groups. The permanent gases were analyzed by MS, which was calibrated for Ar, CH_4, CO, CO_2, and H_2. The solid yield was derived by oxidizing solid residues left in the pyrolyzer at 950 °C in a pure O_2 atmosphere and analyzing the generated CO_2.

2.4. Postexperiment Analysis. The solid residues left after hydropyrolysis were analyzed using a thermogravimetric analyzer (Shimadzu TGA-50). Temperature-programmed oxidations (TPOs) were conducted at a heating rate of 10 °C/min from 30 to 800 °C under air flow with a flow rate of 25 mL/min. The mass changes were recorded, and the derivatives were plotted.

3. RESULTS AND DISCUSSION

3.1. Characterization Results. N_2 adsorption−desorption was conducted for all the materials used in this study; the isotherms and pore size distributions are displayed in Figure 1, while the surface area and pore volume data are shown in Table 1. From the N_2 adsorption−desorption plots, ZSM-5 and Ni-ZSM-5 show typical type I curves, indicating the micropore structures of ZSM-5 and Ni-ZSM-5. MCM-41 shows a typical type IV isotherm, which represents a mesoporous material. Ni-MCM-41 shows both microporosity and mesoporosity, while some of mesoporosity is lost compared to MCM-41. The composites show similar isotherm curves, with both microposority and mesoporosity. The surface area of ZSM-5 was approximately 370 m^2/g and dropped slightly after Ni impregnation while most of the porosity was maintained. MCM-41 showed a very high surface area of 1450 m^2/g with no micropore. The impregnation of MCM-41 by Ni caused a significant decrease of surface area and mesopore volume while the micropore volume was increased. The decrease of surface area and total pore volume might be attributed to partial breakdown of the MCM-41 structure during the impregnation process, which might also cause an increase of the micropore volume. To verify this explanation, we prepared Ni-MCM-41 samples with different Ni loadings (1%−10%). The N_2 adsorption−desorption results (Figure S2 and Table S3 in the SI) demonstrated that all of Ni-MCM-41

https://doi.org/10.1021/acs.energyfuels.1c02453
Energy Fuels 2021, 35, 20117−20130

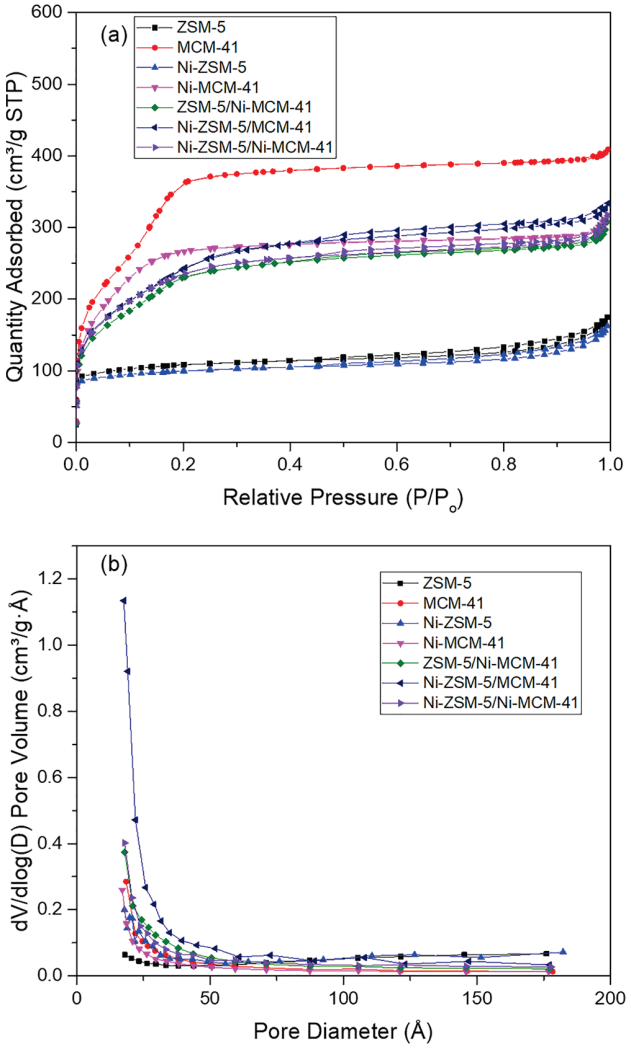

Figure 1. (a) N_2 adsorption−desorption isotherms and (b) pore size distributions of the catalysts used in this study.

Table 1. BET Surface Areas and Pore Volumes of the Catalysts Used in This Study

sample	BET surface area (m^2/g)	micropore volume (cm^3/g)	mesopore volume (cm^3/g)	total pore volume (cm^3/g)
ZSM-5	369	0.114	0.148	0.262
MCM-41	1450	0	0.626	0.626
Ni-ZSM-5	337	0.110	0.132	0.242
Ni-MCM-41	970	0.149	0.324	0.473
ZSM-5/Ni-MCM-41	866	0	0.459	0.459
Ni-ZSM-5/MCM-41	891	0	0.506	0.506
Ni-ZSM-5/Ni-MCM-41	866	0.022	0.452	0.474

samples had a significant decrease of surface area and total pore volume while the micropore volume was increased. The percentage of Ni loading did not significantly affect the surface area, while the small variation should be attributed to the amount of Ni loaded. All the composites showed similar surface areas and total pore volumes, regardless of the location of metal. The surface areas and pore volumes of the composites were higher compared with those of ZSM-5 and lower compared with those of MCM-41, which were in a reasonable range considering the ratio of ZSM-5 and MCM-41 in the composites.

Table 2 shows the ICP-OES results of the actual Ni loading and the Ni dispersion on the catalysts. The results indicate that

Table 2. Ni Loading Percentage of the Catalysts Used in This Study

sample	Ni concentration: measured by ICP-OES (wt %)	Ni concentration: theoretical value (wt %)	Ni dispersion (%)
Ni-ZSM-5	4.92	5	1.00
ZSM-5/Ni-MCM-41	2.32	3.4	6.27
Ni-ZSM-5/MCM-41	1.21	1.6	2.63
Ni-ZSM-5/Ni-MCM-41	4.27	5	7.32
Ni-MCM-41	5.87	5	10.19

Ni was successfully impregnated in the catalysts, and the actual loading percentage was close to the theoretical value. Ni-ZSM-5 showed a dispersion of 1.00%, which suggests that the Ni particle size on ZSM-5 was relatively large. Ni-ZSM-5 encapsulated in MCM-41 showed a higher dispersion than Ni-ZSM-5. Ni-MCM-41 showed a very high metal dispersion of 10.19%, indicating that the Ni nanoparticles were dispersed well on the MCM-41 surface and resulted in a small Ni particle size. ZSM-5/Ni-MCM-41 and Ni-ZSM-5/Ni-MCM-41 both showed a relatively high dispersion, probably due to the deposition of Ni on MCM-41, which would lead to a high dispersion as suggested by Ni-MCM-41.

Figure 2 shows the XRD patterns of the catalysts. MCM-41 is known to have a primary (100) diffraction peak, which was observed at $2\theta = 2.9°$ and corresponds to a d spacing of 3.1 nm.[52] Higher order (110) and (200) peaks were also observed at $2\theta = 5°$ and 5.9°, respectively. All the ZSM-5/MCM-41 composites showed the characteristic (100) diffraction peaks of MCM-41 with slight shifts to the left, which indicates an increased d spacing. The higher angle diffraction data shows that the intrinsic crystal structure of the ZSM-5 remains intact after synthesizing the ZSM-5/MCM-41 composites as the diffraction peaks corresponding to (110), (111), (051), (311), and (323) planes of ZSM-5 are prominent in all the composites. The materials containing reduced Ni nanoparticles showed additional Ni (111) and (200) diffraction peaks at $2\theta = 44.5°$ and 51.8°, respectively.

The SEM and TEM images of all catalysts are presented in Figure 3. Parts a and b of Figure 3 show the morphology of bare MCM-41, which is a micron-level sphere with ordered mesopores. The Ni-ZSM-5 has a smaller particle size compared to MCM-41, which suggests that the encapsulation of Ni-ZSM-5 in MCM-41 is feasible. From the TEM image of Ni-ZSM-5 shown in Figure 3d, the Ni nanoparticles can be clearly observed on the ZSM-5 surface. Parts e and f of Figure 3 show the SEM and TEM images of Ni-MCM-41, respectively. The SEM image shows that the Ni nano particles are well-dispersed on the MCM-41 surface, which is consistent with the TEM images. Large Ni particles are also observed. The composite Ni-ZSM-5/MCM-41 (Figure 3g,h) shows a very similar morphology to MCM-41, while some deformation of the particles was observed on their surfaces, which should be attributed to the encapsulation of Ni-ZSM-5. Such deformation has been observed and explained in our previous study.[19] No apparent Ni nanoparticles were observed on the outer

https://doi.org/10.1021/acs.energyfuels.1c02453
Energy Fuels 2021, 35, 20117−20130

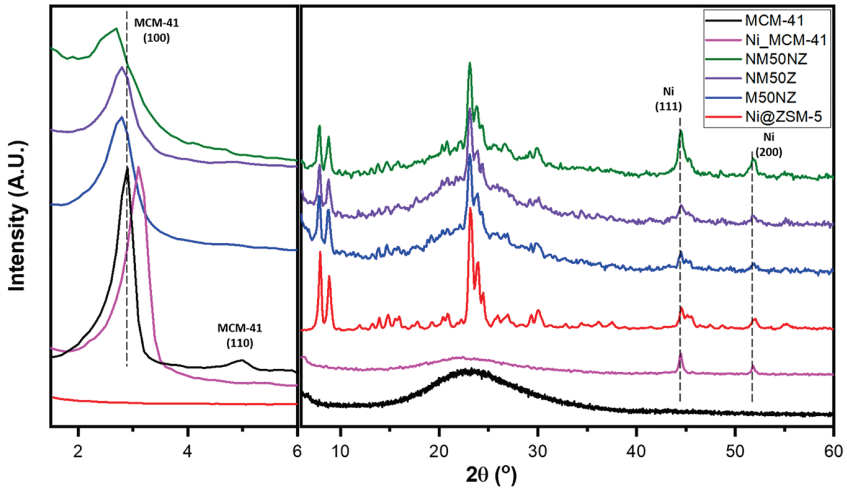

Figure 2. XRD patterns of the catalysts used in this study.

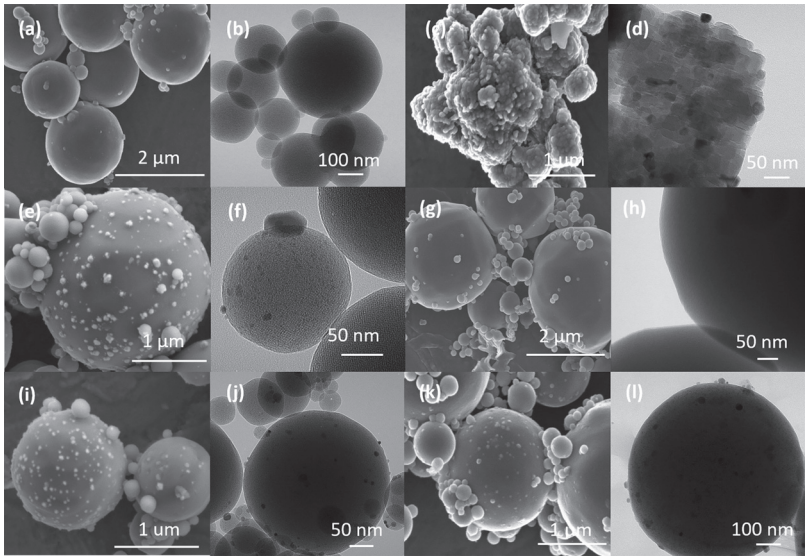

Figure 3. SEM and TEM images of the catalysts: (a and b) MCM-41, (c and d) Ni-ZSM-5, (e and f) Ni-MCM-41, (g and h) Ni-ZSM-5/MCM-41, (i and j) ZSM-5/Ni-MCM-41, and (k and l) Ni-ZSM-5/Ni-MCM-41.

surface of the composite, suggesting that the Ni-ZSM-5 particles were successfully covered by the MCM-41 layer. The composites ZSM-5/Ni-MCM-41 and Ni-ZSM-5/Ni-MCM-41 in Figure 3i–l show similar surface morphologies to Ni-MCM-41, which is expected. The Ni nanoparticles are also observed on the surfaces of both composites.

3.2. One-Stage CFHP with or without Hydrotreatment. *Scenario 1: One-Stage CFHP Using Ni-ZSM-5 (Control Experiment).* The one-stage CFHP was first performed at 600 and 500 °C using Ni-ZSM-5, and the results are displayed in Figures 4 and 5, respectively. Figures 4a and 5a show the overall product yields, Figures 4b and 5b show the gas product distribution, and Figures 4c and 5c show the liquid product distribution. Detailed alkane selectivity can be found in Figure S6 of the SI. We want to emphasize that the liquid product yields in this study are low compared to ours and others published studies.[39,41,45,47] This is mainly attributed to the fact that we have used a relatively low catalyst to biomass ratio. Note that in this study the Ni-ZSM-5/biomass ratio is maintained at 1.6:1. We used this ratio to maintain the same amount of Ni-ZSM-5 in all our experiments. Thus, the comparison of the performance of the composites would be on the same basis, that is, the amount of zeolite used. If we have increased the Ni-ZSM-5/biomass ratio to 5:1 (a more typical ratio), the liquid carbon yield would be approximately 30% (comparable with the literature).[24,33] However, to compare the aforementioned Ni-ZSM-5 performance with the performance of composites, we should have applied a composite/biomass ratio of 15.6:1. At this high catalyst to biomass ratio, the methanation reaction is so significant that the products are mainly gases (methane). Thus, we decided to present our results at a low catalyst to biomass ratio to properly convey our concepts.

Using Ni-ZSM-5 at 600 °C, the total gas and solid carbon yields were both close to 40%, while the total liquid yield was only approximately 13%, which might be attributed to the low C/B ratio. The major liquid products produced by Ni-ZSM-5 were monoaromatic hydrocarbons (MAH), including benzene, toluene, xylene, alkyl benzenes, and indenes, with approximately 9.4% yield on a feed carbon basis. Approximately 1.5%

https://doi.org/10.1021/acs.energyfuels.1c02453
Energy Fuels 2021, 35, 20117–20130

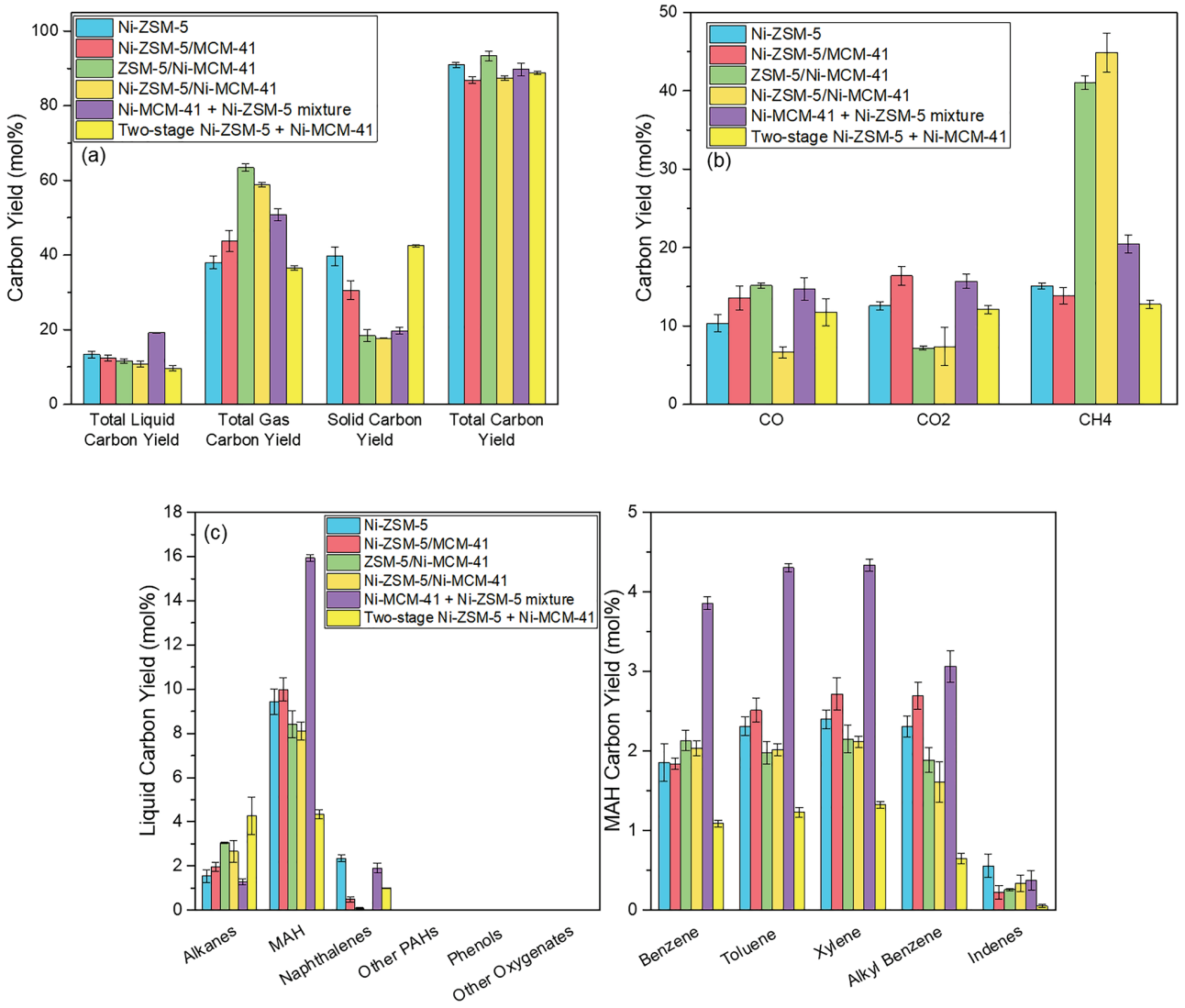

Figure 4. CFHP with/without hydrotreatment at 600 °C: (a) overall carbon yield, (b) gas carbon yields, and (c) liquid product distribution.

carbon yield to alkanes and 2.3% carbon yield to naphthalenes were observed. No oxygenates were found in the liquid products in these CFHP experiments. This is advantageous compared to the CFP experiments using ZSM-5, where oxygenates are observed in the liquid products.[19] The results suggest that CFHP leads to a hydrocarbon-rich liquid bio-oil without oxygenates compared to CFP. In gas products, the CH_4 yield was significantly promoted, compared to CFP,[19] which was consistent with our previous study.[35] This suggests that the methanation reaction was dramatically enhanced in CFHP using Ni-ZSM-5.

At 500 °C, Ni-ZSM-5 showed an inferior performance compared to the results at 600 °C. Almost no alkanes and fewer MAH and naphthalenes were found in the liquid product pool (MAH yield dropped from 9.4% to 6.2%). The naphthalenes yield was also much lower at 500 °C, probably due to insufficient cracking and deoxygenation reactions at this lower temperature. The solid yield increased significantly from 40% to 56%. Higher solid and lower CO_2 yields indicate that the deoxygenation reaction was suppressed at 500 °C. The methanation reaction was also restrained as less methane was formed. Interestingly, the CO yield at 500 °C was significantly higher than at 600 °C; this might be attributed to the following: (1) A higher CFHP temperature can result in a higher water yield,[36] which might alter the deoxygenation reactions from decarbonylation to dehydration reaction; (2) CO might react with H_2 during CFHP in the presence of Ni catalysts, leading to the formation of CH_4 and H_2O. This reaction is temperature sensitive and is intensified at a higher temperature,[53] which will result in a lower CO yield and a higher methane yield. Comparing the results of Ni-ZSM-5 at 600 and 500 °C, it can be concluded that a higher pyrolysis temperature is preferred for the production of more MAH and alkanes and fewer solids.

Scenario 2: (a) One-Stage CHFP and Hydrotreatment Using Ni-ZSM-5/MCM-41 - The Role of MCM-41 Layer on Ni-ZSM-5. The objective of these experiments was to understand the role of the MCM-41 layer on the Ni-ZSM-5 catalyst on the cracking and hydrotreatment reactions of the hydropyrolysis vapors. The results at 600 and 500 °C are shown in Figures 4 and 5, respectively. At 600 °C, the Ni-ZSM-5/MCM-41 composite showed a very similar total liquid carbon yield to Ni-ZSM-5, whereas the total gas yield was increased and the solid yield was decreased compared to those of Ni-ZSM-5. The

https://doi.org/10.1021/acs.energyfuels.1c02453
Energy Fuels 2021, 35, 20117−20130

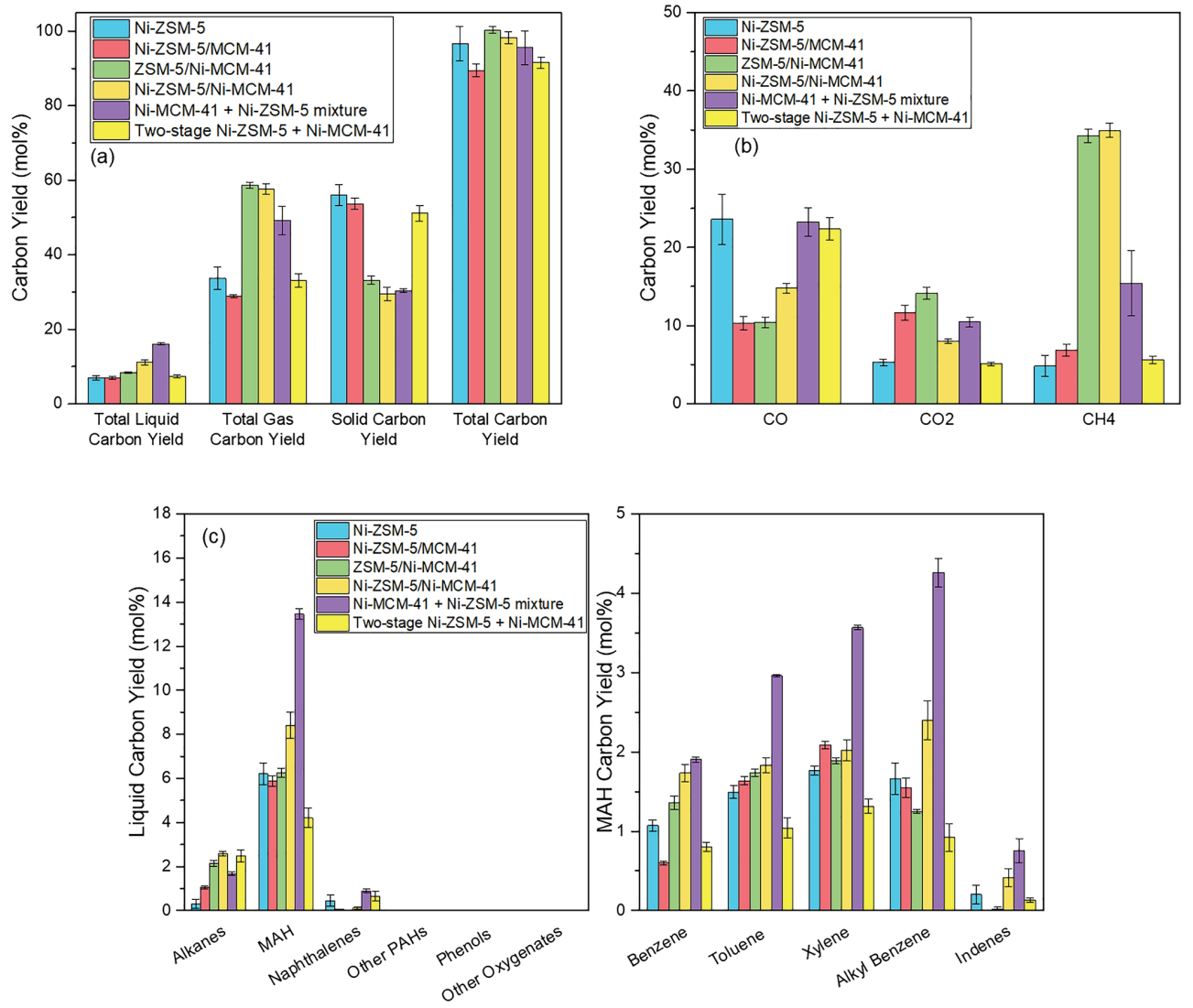

Figure 5. CFHP with/without hydrotreatment at 500 °C: (a) overall carbon yield, (b) gas carbon yields, and (c) liquid product distribution.

solid carbon yield dropped to 30%, which was a substantial reduction compared to that of Ni-ZSM-5. Ni-ZSM-5/MCM-41 also showed a small increase of MAH and alkanes yields, compared to the results of Ni-ZSM-5. However, the naphthalenes yield dropped. This might contribute to the slight increase of MAH and alkane yields, as MCM-41 might cover the external acid sites of ZSM-5, inhibiting the polymerization reaction on the external surface of ZSM-5 and reducing the yield of naphthalenes and coke.[54] The increase of CO and CO_2 yields indicated stronger deoxygenation reactions with the additional MCM-41 layer compared to those of Ni-ZSM-5, which might also explain the decrease of solid yield.

At 500 °C, the Ni-ZSM-5/MCM-41 composite also showed a similar total liquid carbon yield compared to Ni-ZSM-5. However, the Ni-ZSM-5/MCM-41 composite showed a higher alkane yield and a lower benzene yield than Ni-ZSM-5 at 500 °C. The solid carbon yield by Ni-ZSM-5/MCM-41 showed a small decrease compared to that of Ni-ZSM-5, which was not as significant as at 600 °C. The CO yield using Ni-ZSM-5 was much higher compared to that of Ni-ZSM-5/MCM-41, which might be attributed to the direct contact of Ni-ZSM-5 and biomass in the absence of the MCM-41 layer. MCM-41 does not promote decarbonylation reaction at the extent that ZSM-5 does.[19] Thus, the coverage of Ni-ZSM-5 by MCM-41 might lead to a lower CO yield. Nevertheless, more CO_2 and CH_4 were produced by Ni-ZSM-5/MCM-41 compared to with Ni-ZSM-5. The results at 600 and 500 °C by Ni-ZSM-5/MCM-41 indicate that a relatively higher temperature is beneficial for increasing liquid yield and decreasing solid yield, as well as enhancing the production of alkanes. In conclusion, it appears that the presence of the MCM-41 layer covered the external acid sites of ZSM-5, inhibiting the polymerization reactions on the external surface of ZSM-5 and reducing the yield of naphthalene and coke. The comparison between the Ni-ZSM-5/MCM-41 composite and Ni-ZSM-5 also proved that Ni-ZSM-5 in the composite was totally accessible, which is consistent with our previous study.[19]

Scenario 2: (b) One-Stage CFHP and Hydrotreatment Using ZSM-5/Ni-MCM-41 - The Role of Ni on the MCM-41 Layer. The objective of these experiments was to better understand the role of Ni on cracking and hydrotreatment reactions on the MCM-41 layer. The results at 600 and 500 °C are shown in Figures 4 and 5, respectively. When the ZSM-5/

https://doi.org/10.1021/acs.energyfuels.1c02453
Energy Fuels 2021, 35, 20117−20130

Ni-MCM-41 composite was used as a catalyst at 600 °C, the total liquid carbon yield was similar to those of Ni-ZSM-5 and Ni-ZSM-5/MCM-41. However, the total gas yield was further ascended and solid yield was further descended compared to tose of Ni-ZSM-5/MCM-41. The significant increase of total gas yield was mainly attributed to the drastic increase of CH_4. The high yield of CH_4 was likely due to the presence of Ni on the MCM-41 surface. In our previous study, we have also demonstrated that Ni-SiO_2 leads to higher CH_4 and lower solid yields compared to Ni-ZSM-5.[44] MCM-41 and SiO_2 have similar elemental compositions, thus we should expect a similar effect on methanation reactions. The results by ZSM-5/Ni-MCM-41 and Ni-SiO_2 imply that the direct contact of biomass with Ni-MCM-41 can shift the yield of less-valued solids to higher-valued methane, which could be a useful gas in the integrated hydropyrolysis and hydrotreatment process. Methane can be used for the production of hydrogen by steam reforming, thus allowing for a continuous and self-sustained process.[39,40] Notably, the alkane yield by ZSM-5/Ni-MCM-41 was increased to 3%, while the MAH yield slightly dropped. These results indicate that the Ni-MCM-41 layer resulted in the hydrogenation of MAH to alkanes, which is consistent with our hypothesis that the deoxygenated liquid products can be hydrotreated on the Ni-MCM-41 outer layer of the composite immediately after they exit the ZSM-5. Thus, this result indicates that the two-stage hydropyrolysis and hydrotreatment in one catalytic particle could be feasible.

The results of one-stage CFHP and hydrotreatment using ZSM-5/Ni-MCM-41 at 500 °C showed a similar trend to the results at 600 °C. A further increase of alkane yield (compared to Ni-ZSM-5/MCM-41) was obtained using ZSM-5/Ni-MCM-41, while the MAH yield was basically maintained compared to Ni-ZSM-5. That was a different observation compared to the experiments at 600 °C, where a slight decrease of MAH yield was observed. Stronger methanation reactions and a lower solid yield were also observed at this temperature using ZSM-5/Ni-MCM-41, which was consistent with the results at 600 °C. These results suggest that Ni on the MCM-41 layer of the composite leads to stronger hydrogenation activity, compared to Ni on ZSM-5. Ni-MCM-41 can also promote methanation reactions.

Scenario 2: (c) One-Stage CFHP and Hydrotreatment Reactions Using the Ni-ZSM-5/Ni-MCM-41 Composite - Exploring a Better Composite Material. The objective of these experiments was to understand whether the Ni-ZSM-5/Ni-MCM-41 composite is a better candidate for the one-stage CFHP and hydrotreatment experiments compared to Ni-ZSM-5/MCM-41 and ZSM-5/Ni-MCM-41. All the results at 600 and 500 °C are shown in Figures 4 and 5, respectively. The performance of Ni-ZSM-5/Ni-MCM-41 at 600 °C was similar to that of ZSM-5/Ni-MCM-41, except that even stronger methanation reactions were observed and less CO was formed with the former composite. The lower CO yield suggested that the decarbonylation reactions were suppressed, leading to a lower hydrocarbon yield. However, methanation reactions were catalyzed in the presence of Ni on ZSM-5. It is well-known in the literature that Ni catalyzes these reactions.[41,55,56]

Comparing the results at 600 and 500 °C, it appears that a higher temperature promoted methanation reactions and suppressed the production of solids, while the liquid yields were not significantly affected. The alkanes and MAH yields by Ni-ZSM-5/Ni-MCM-41 were similar at 500 and 600 °C, indicating that the deoxygenation and hydrotreatment reactions were not greatly impacted by the change of pyrolysis temperature. Nevertheless, lower methane and higher solid yields were observed at 500 °C compared to those at 600 °C. Compared to other composites, Ni-ZSM-5/Ni-MCM-41 showed the least impact on liquid product distribution under the influence of temperature, which implies that such composite might be applicable at a wider range of operating temperature of CFHP.

Scenario 3: One-Stage CFHP Followed by Hydrotreatment Using the Physical Mixture of Ni-MCM-41 and Ni-ZSM-5 - Understanding the Role of Composite Structure. To understand the importance of the structure of composite (i.e., the encapsulation of Ni-ZSM-5 in Ni-MCM-41), we performed one-stage experiments using the physical mixture of Ni-MCM-41 and Ni-ZSM-5 at both 600 and 500 °C. The results are presented in Figures 4 and 5. It appears that, at 600 °C, the physical mixture showed a much higher total liquid yield and a lower total gas yield than the Ni-ZSM-5/Ni-MCM-41 composite and approximately the same solid yield. The increase of liquid carbon yield was mainly attributed to MAH, which reached 16% of carbon yield. However, the alkanes yield using the physical mixture was lower than using the composite. The CH_4 yield was remarkably lower using the physical mixture, while the CO and CO_2 yields were higher.

The product distribution at 500 °C by the physical mixture was very similar to that at 600 °C. A lower liquid yield and a higher solid yield were observed at 500 °C. The MAH yield dropped from 16% to 13.5% as the temperature decreased from 600 to 500 °C. Interestingly, the alkane yield did not decrease with the decrease of temperature as in the case of Ni-ZSM-5. Instead, it increased slightly. This might be attributed to the lower temperature, which favors hydrogenation reactions in the presence of Ni-MCM-41. Thus, when the temperature dropped from 600 to 500 °C, the alkane yield increased using the physical mixture. However, the alkane yield (1.7%) produced by physical mixture was not as high as the alkane yield (2.6%) produced by the Ni-ZSM-5/Ni-MCM-41 composite. These results suggest that the composite structure allows for stronger hydrogenation and methanation reactions. This might be attributed to the direct contact of Ni-MCM-41 and biomass, which leads to the production of a higher methane yield, while fewer vapors are generated and contact with Ni-ZSM-5 inside the catalyst particle. As fewer pyrolysis vapors are generated, the MAH yield is reduced. Therefore, it appears that the composite and the mixture come with their own benefits: the composite produces more alkanes in the hydrocarbon pool and substantially increases the yields to methane in the expense of aromatics. That methane can be used for the production of renewable hydrogen through reforming reactions leads to a sustainable process, which relies solely on renewable resources. On the contrary, the physical mixture provides a high selectivity to MAH in the hydrocarbon pool. As the high yield of methane caused by Ni-MCM-41 might be the reason for the relatively low yield of MAH by the Ni-ZSM-5/Ni-MCM-41 composite, optimizing the ratio of Ni-ZSM-5 and Ni-MCM-41 in the composite as well as the amount of Ni in MCM-41 and ZSM-5 might improve the total liquid carbon yield and obtain the same or higher MAH yield compared to the physical mixture.

Summarizing One-Stage CHFP Experimental Results. Summarizing, at 600 °C, Ni-ZSM-5 leads to the production of alkanes, MAH, and naphthalenes in the liquid products with no oxygenates and a considerable amount of solids. The

https://doi.org/10.1021/acs.energyfuels.1c02453
Energy Fuels 2021, 35, 20117−20130

additional MCM-41 layer on Ni-ZSM-5 (Ni-ZSM-5/MCM-41 composite) slightly increased the yield to MAH and alkanes at the expense of naphthalenes and solids. ZSM-5/Ni-MCM-41 and Ni-ZSM-5/Ni-MCM-41 showed very similar results. Both composites promoted the production of alkanes at the expense of MAH, most likely due to the presence of Ni on MCM-41. The most apparent effect was the substantial enhancement of methanation reactions and the reduction of solids due to the presence of Ni on the surface of MCM-41. The Ni-MCM-41 and Ni-ZSM-5 physical mixture resulted in the highest MAH yields than any other catalysts. However, the hydrogenation and methanation reactions were suppressed, which led to a lower alkane yield and a significantly lower methane yield compared to the Ni-ZSM-5/Ni-MCM-41 composite. The results at 500 °C showed an overall lower total liquid carbon yield and higher solid yield for all the catalysts compared to the results derived at 600 °C. The methanation reactions were also suppressed at a lower temperature, as indicated by the lower yield of methane. From the experimental data, we do not expect that CO_2, CO, and/or CH_4 have reached equilibrium concentration though reverse water gas shift or methanization reaction for any of the catalysts used. Some relevant calculations are shown in the SI. The effect of Ni was also evaluated by performing CFHP experiments at 600 °C using MCM-41, ZSM-5, and their physical mixture. The results and corresponding discussion can be found in the SI.

In our previous study,[41] we used a two-stage reaction system where *Miscanthus* was hydropyrolized using Ni-ZSM-5 at the first stage and the vapors were then hydrotreated using Ni-SiO_2 at the second stage. The results demonstrated that the second-stage hydrotreatment shifted the yield of MAH to alkanes without affecting any other product distribution. The major difference between Ni-ZSM-5/Ni-MCM-41 and the two-stage system mentioned above is that the former not only enhanced the selectivity to alkanes but also reduced the solid yield and formed CH_4. Thus, our results suggest that a two-stage catalytic hydropyrolysis and hydrotreatment process is feasible using only one catalyst particle. To further strengthen the feasibility of one-stage hydropyrolysis and hydrotreatment reaction in one sole catalyst particles (i.e., Ni-ZSM-5/Ni-MCM-41) we also performed two-stage experiments with Ni-ZSM-5 in the first CFHP step and the Ni-MCM-41 in the second hydrotreatment stage. The results are discussed in the section below.

3.3. Two-Stage CFHP and Hydrotreatment Using Ni ZSM-5 and Ni-MCM-41 (Scenario 4). To better understand whether the two reactions of hydropyrolysis and hydrotreating can be integrated in a one-step catalytic process, we performed two-stage experiments where Ni-ZSM-5 was in the first hydropyrolysis stage and Ni-MCM-41 was in a separate downstream hydrotreatment reactor. The experiments were conducted with the temperatures of the first CFHP stage at 600 and 500 °C and the second hydrotreatment stage at 300 °C. The results are shown in Figures 4 and 5 for 600 and 500 °C, respectively. At both pyrolysis temperatures, the gas product distribution and the solid yield of the two-stage experiments were very similar to the results using Ni-ZSM-5 alone, which was expected. When the CFHP temperature was at 600 °C, a considerable amount of MAH was converted to alkanes as expected. The carbon yield of alkanes at 600 °C in the two-stage process was higher compared to those of all the other one-stage experiments. However, that was not the case at 500 °C. At 500 °C, the two-stage process showed almost the same alkane yield to the one-stage process using the Ni-ZSM-5/Ni-MCM-41 composite. Notice also that the one-stage process using the Ni-ZSM-5/Ni-MCM-41 composite led to a significantly higher MAH yield compared to the two-stage process, which can be a major advantage of the Ni-ZSM-5/Ni-MCM-41 composite. Another worth noticing observation was that the distribution of alkanes by the one-stage and the two-stage processes at 500 °C was different. The alkanes produced by the one-stage Ni-ZSM-5/Ni-MCM-41 were mainly cyclohexanes and cyclopentanes, while in the case of the two-stage process, the alkanes were composed mainly of cyclohexanes and decalins. This difference suggests that the direct contact of Ni-MCM-41 and biomass will result in additional cracking, which can lead to the production of C_5 species. This conclusion is also supported by the difference in the MAH yields; the MAH yield using Ni-ZSM-5/Ni-MCM-41 was much higher than those using Ni-ZSM-5 alone or with Ni-MCM-41 in the second stage. Therefore, additional hydrocarbons were produced with the assistance of the Ni-MCM-41 layer of the composite. In addition, the two-stage process resulted in substantially higher solids and substantially lower methane yields, which was a significant advantage of the one-stage process using the composite. These results clearly demonstrate that the composites can successfully complete the two-step CFHP and hydrotreatment reactions in one, single step, allowing also for significant methane production, which can be used for the production of the needed hydrogen. A lower pyrolysis temperature also favors the one-stage process using the composite.

3.4. Postexperiment Analysis Results. To understand the effects of different composites on the properties of solid products, temperature-programmed oxidations of the solid residue were performed. The DTG curves at a temperature range of 200−800 °C are displayed in Figure 6. The solid residue by Ni-ZSM-5 showed a small peak at 330 °C and a broad peak from 400 to 600 °C, with a shoulder at approximately 530 °C. The solid residue by the Ni-ZSM-5/Ni-MCM-41 composite showed a major peak at 450 °C and a small peak at 550 °C. The solid residue by the Ni-MCM-41 and Ni-ZSM-5 mixture showed a broad peak from 300 to 500

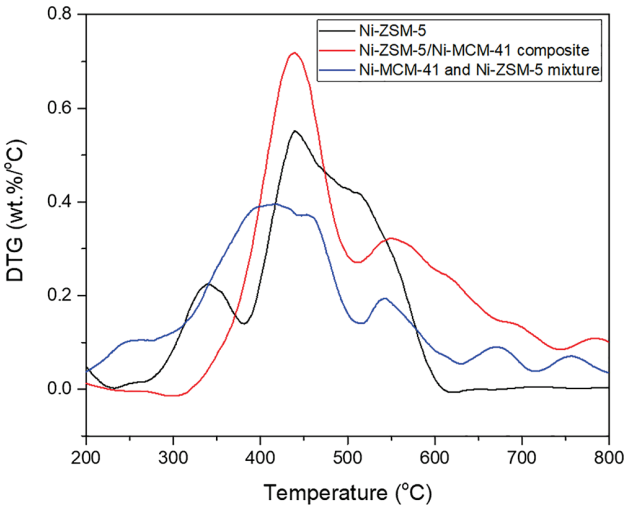

Figure 6. DTG curves of temperature-programmed oxidation of solid residue by CFHP at 500 °C using different catalysts.

https://doi.org/10.1021/acs.energyfuels.1c02453
Energy Fuels 2021, 35, 20117−20130

°C with a small peak at 550 °C, as well. The peaks below 500 °C are typically attributed to char, while the peak at 550 °C is typically attributed to coke. The oxidation temperature of char can reflect its properties; a lower oxidation temperature suggests that the char is rich in oxygen content with a lower degree of decomposition.[57] The appearance of the oxidation peak of Ni-ZSM-5 at 330 °C indicates that Ni-ZSM-5 was not active enough to crack and decompose *Miscanthus*, which caused the high solid yield during the CFHP experiments. The Ni-ZSM-5/Ni-MCM-41 composite showed distinct peaks of char and coke with the appearance of the char peak at a relatively high oxidation temperature, which implies that the biomass was completely decomposed and the yields of liquid and gas products were maximized. The physical mixture of Ni-MCM-41 and Ni-ZSM-5 also showed characteristic peaks of char and coke. The coke peak appeared at the same oxidation temperature as for the Ni-ZSM-5/Ni-MCM-41 composite. However, the char peak shifted to a lower temperature. As discussed in the previous section, the yields of solid produced by the composite and the physical mixture were approximately equal, while the physical mixture produced more liquid and less gas (specifically less methane) than the composite. Thus, the different oxidation temperatures of the residue char derived by the composite and the physical mixture might be due to the methanation reactions. The composite promoted methanation reactions, which contributed to a deeper degree of *Miscanthus* decomposition and caused the increase of the oxidation temperature of the char. The decomposition of *Miscanthus* by the composite was mainly attributed to methanation reactions, as well as the hydrocracking of large biopolymers. However, the methanation reactions were suppressed by the physical mixture, as less biomass was able to contact with Ni-MCM-41 particles due to the exposure of Ni-ZSM-5 to biomass. As a result, fewer pyrolysis vapors were generated using the composite that led to a lower total liquid yield compared to the physical mixture. These results prove that the layer of the Ni-MCM-41 on the composite structure significantly changed the composition of gas, liquid, and solid products. Although we anticipate that the proposed composites will have a higher lifetime due to the sacrificial act of the MCM-41 layer,[19] regeneration of the composites will be necessary for a continuous operation. Therefore, a reactor setup similar to the fluid catalytic cracking unit (riser and regenerator) might be appropriate.

4. CONCLUSIONS

In this study, the feasibility of realizing tandem reactions using a single, composite catalyst has been explored. Specifically, we studied the combination of the two-step CFHP and hydrotreating process in one step, within one catalyst particle. The ZSM-5/MCM-41 composites with Ni loaded on MCM-41 and/or ZSM-5 were prepared. The characterization results indicated that the composites were successfully prepared and Ni was successfully impregnated into the composites at different locations (on MCM-41 surface and/or ZSM-5 surface). The one-step CFHP and hydrotreatment experiments at 600 and 500 °C showed that the MCM-41 layer over Ni-ZSM-5 did not significantly affect the yield of MAH and alkanes compared to with Ni-ZSM-5 alone. With the impregnation of Ni on MCM-41, the alkane yields were increased and the methanation reactions were drastically enhanced. The comparison between the results derived at CFHP temperatures of 600 and 500 °C verified that a higher pyrolysis temperature was beneficial to the production of MAH and methane. This might be attributed to the fact that a higher temperature favors aromatics production due to thermodynamics. However, we should keep in mind that although higher temperatures might shift the equilibrium between aromatics and alkanes toward the production of aromatics, the alkanes yield was also higher at 600 °C compared to that at 500 °C. The higher yields of all liquid products at a higher temperature might be attributed to the higher reaction rates, which allowed more solids to be converted into valuable liquid products. The product distribution was the least impacted by the temperature using the Ni-ZSM-5/Ni-MCM-41 composite. The experiments at 500 °C using Ni-ZSM-5 and Ni-ZSM-5/Ni-MCM-41 composite showed clear evidence that the composite promoted alkane production. At 500 °C, the one-stage CFHP and hydrotreatment experiments using Ni-ZSM-5/Ni-MCM-41 showed similar alkane and much higher MAH yield compared to the two-stage process where Ni-ZSM-5 and Ni-MCM-41 were placed in separate reactors. Interestingly, the Ni-MCM-41 and Ni-ZSM-5 physical mixture showed the highest yield in MAH, which will be the preferred choice if the liquid aromatics are the desired product. However, clear evidence has shown that the Ni-ZSM-5/Ni-MCM-41 composite was able to produce more alkanes than the physical mixture, suggesting that the composite structure is the catalyst that promotes the production of alkanes in a one-stage reactor. Therefore, this study has indicated that a one-step CFHP and hydrotreating step is feasible using the Ni-ZSM-5/Ni-MCM-41 composite. One of the most important results of the study was that the one-step process using the composite can significantly increase the production of methane while minimizing the solids. The produced methane can be utilized for the *in situ* production of renewable hydrogen, making this process fully self-sustainable. Water gas shift reaction during the CFHP can also generate additional hydrogen. However, we also noticed that the high methanation yield might have caused low total liquid carbon yield and MAH yield. Hence, future work will focus on optimizing the ratio of Ni-ZSM-5 and Ni-MCM-41 in the composite, the amount of Ni on MCM-41 and ZSM-5, and the experimental conditions to avoid strong methanation reactions and therefore maximize the total liquid carbon yield to MAH yield, as well as alkanes.

■ ASSOCIATED CONTENT

Supporting Information

The Supporting Information is available free of charge at https://pubs.acs.org/doi/10.1021/acs.energyfuels.1c02453.

Tables of proximate analysis and ultimate analysis of miscanthus, mass of biomass and catalyst used in each scenario, BET surface areas and pore volumes of MCM-41 impregnated by different amounts of Ni, and concentrations of Brønsted and Lewis acid sites and their ratio of each catalyst and figures of schematic showing the spray drying setup for catalyst synthesis, N_2 adsorption−desorption isotherms, pore size distributions, Ni particle size distribution of the various catalysts, DRIFTS spectra, catalytic and noncatalytic fast hydropyrolysis at 600 °C, alkane selectivity at pyrolysis temperatures of 600 and 500 °C, equilibrium calculation of reverse water gas shift reaction and methanation reactions during CFHP experiments (PDF)

https://doi.org/10.1021/acs.energyfuels.1c02453
Energy Fuels 2021, 35, 20117−20130

AUTHOR INFORMATION

Corresponding Authors

Vijay T. John − *Department of Chemical & Biomolecular Engineering, Tulane University, New Orleans, Louisiana 70118, United States;* orcid.org/0000-0001-5426-7585; Phone: +1 504 865 5883; Email: vj@tulane.edu

Julia A. Valla − *Department of Chemical and Biomolecular Engineering, University of Connecticut, Storrs, Connecticut 06269, United States;* orcid.org/0000-0002-4402-0818; Phone: +30 617 633 2157; Email: ioulia.valla@uconn.edu

Authors

Lei Yu − *Department of Chemical and Biomolecular Engineering, University of Connecticut, Storrs, Connecticut 06269, United States;* orcid.org/0000-0003-0119-4452

Azeem Farinmade − *Department of Chemical & Biomolecular Engineering, Tulane University, New Orleans, Louisiana 70118, United States;* orcid.org/0000-0003-1343-9496

Oluwole Ajumobi − *Department of Chemical & Biomolecular Engineering, Tulane University, New Orleans, Louisiana 70118, United States;* orcid.org/0000-0003-4356-7923

Complete contact information is available at: https://pubs.acs.org/10.1021/acs.energyfuels.1c02453

Author Contributions

[§]L.Y. and A.F.: equal first author contribution.

Notes

The authors declare no competing financial interest.

ACKNOWLEDGMENTS

This work was supported by the National Science Foundation (NSF grant number: CMMI 1826146).

REFERENCES

(1) Wu, L.; Xue, X.; Yu, H.; Zhang, C.; Wei, X.; Liang, J.; Sun, Y. Catalytic Pyrolysis of Poplar Sawdust: Excellent Hydrocarbon Selectivity and Activity of Hollow Zeolites. *Bioresour. Technol.* **2020**, *317* (May), 123954.

(2) Zou, R.; Wang, Y.; Jiang, L.; Yu, Z.; Zhao, Y.; Wu, Q.; Dai, L.; Ke, L.; Liu, Y.; Ruan, R. Microwave-Assisted Co-Pyrolysis of Lignin and Waste Oil Catalyzed by Hierarchical ZSM-5/MCM-41 Catalyst to Produce Aromatic Hydrocarbons. *Bioresour. Technol.* **2019**, *289* (June), 121609.

(3) Kumar, A.; Kumar, A.; Kumar, J.; Bhaskar, T. Catalytic Pyrolysis of Soda Lignin over Zeolites Using Pyrolysis Gas Chromatography-Mass Spectrometry. *Bioresour. Technol.* **2019**, *291* (May), 121822.

(4) Resende, F. L. P. Recent Advances on Fast Hydropyrolysis of Biomass. *Catal. Today* **2016**, *269*, 148−155.

(5) Venkatesan, K.; Prashanth, F.; Kaushik, V.; Choudhari, H.; Mehta, D.; Vinu, R. Evaluation of Pressure and Temperature Effects on Hydropyrolysis of Pine Sawdust: Pyrolysate Composition and Kinetics Studies. *React. Chem. Eng.* **2020**, *5* (8), 1484−1500.

(6) Hu, C.; Liu, C.; Liu, Q.; Zhang, H.; Wu, S.; Xiao, R. Effects of Steam to Enhance the Production of Light Olefins from ex situ Catalytic Fast Pyrolysis of Biomass. *Fuel Process. Technol.* **2020**, *210* (June), 106562.

(7) Chen, W. H.; Lin, B. J.; Huang, M. Y.; Chang, J. S. Thermochemical Conversion of Microalgal Biomass into Biofuels: A Review. *Bioresour. Technol.* **2015**, *184*, 314−327.

(8) Ong, H. C.; Chen, W. H.; Farooq, A.; Gan, Y. Y.; Lee, K. T.; Ashokkumar, V. Catalytic Thermochemical Conversion of Biomass for Biofuel Production: A Comprehensive Review. *Renewable Sustainable Energy Rev.* **2019**, *113* (July), 109266.

(9) Yu, L.; Gamliel, D. P.; Markunas, B.; Valla, J. A. A Promising Solution for Food Waste: Preparing Activated Carbons for Phenol Removal from Water Streams. *ACS Omega* **2021**, *6* (13), 8870−8883.

(10) Xue, S.; Luo, Z.; Wang, W.; Li, S.; Sun, H.; Zhou, Q.; Liang, X. Preparation of Aromatics from Catalytic Pyrolysis of Enzymatic Lignin over Double-Layer Metal Supported Core-Shell Catalyst. *J. Anal. Appl. Pyrolysis* **2020**, *150* (March), 104884.

(11) Xue, X.; Wu, L.; Wei, X.; Liang, J.; Sun, Y. Product Modification in Catalytic Fast Pyrolysis of Corn Stalk: The Decoupled Effect of Acidity and Porosity within a Core-Shell Micro-/Mesoporous Zeolite. *ACS Sustainable Chem. Eng.* **2020**, *8* (19), 7445−7453.

(12) Gamliel, D. P.; Karakalos, S.; Valla, J. A. Liquid Phase Hydrodeoxygenation of Anisole, 4-Ethylphenol and Benzofuran Using Ni, Ru and Pd Supported on USY Zeolite. *Appl. Catal., A* **2018**, *559*, 20−29.

(13) Gamliel, D. P.; Baillie, B. P.; Augustine, E.; Hall, J.; Bollas, G. M.; Valla, J. A. Nickel Impregnated Mesoporous USY Zeolites for Hydrodeoxygenation of Anisole. *Microporous Mesoporous Mater.* **2018**, *261*, 18−28.

(14) Du, S.; Valla, J. A.; Bollas, G. M. Characteristics and Origin of Char and Coke from Fast and Slow, Catalytic and Thermal Pyrolysis of Biomass and Relevant Model Compounds. *Green Chem.* **2013**, *15* (11), 3214−3229.

(15) Ma, S.; Li, H.; Zhang, G.; Iqbal, T.; Li, K.; Lu, Q. Catalytic Fast Pyrolysis of Walnut Shell for Alkylphenols Production with Nitrogen-Doped Activated Carbon Catalyst. *Front. Environ. Sci. Eng.* **2021**, *15* (2), 25.

(16) Du, S.; Gamliel, D. P.; Valla, J. A.; Bollas, G. M. The Effect of ZSM-5 Catalyst Support in Catalytic Pyrolysis of Biomass and Compounds Abundant in Pyrolysis Bio-Oils. *J. Anal. Appl. Pyrolysis* **2016**, *122*, 7−12.

(17) Gamliel, D. P.; Du, S.; Bollas, G. M.; Valla, J. A. Investigation of in Situ and Ex Situ Catalytic Pyrolysis of Miscanthus × Giganteus Using a PyGC-MS Microsystem and Comparison with a Bench-Scale Spouted-Bed Reactor. *Bioresour. Technol.* **2015**, *191*, 187−196.

(18) Gamliel, D. P.; Cho, H. J.; Fan, W.; Valla, J. A. On the Effectiveness of Tailored Mesoporous MFI Zeolites for Biomass Catalytic Fast Pyrolysis. *Appl. Catal., A* **2016**, *522*, 109−119.

(19) Yu, L.; Farinmade, A.; Ajumobi, O.; Su, Y.; John, V. T.; Valla, J. A. MCM-41/ZSM-5 Composite Particles for the Catalytic Fast Pyrolysis of Biomass. *Appl. Catal., A* **2020**, *602* (June), 117727.

(20) Chen, Z.; Zhang, X.; Yang, F.; Peng, H.; Zhang, X.; Zhu, S.; Che, L. Deactivation of a Y-Zeolite Based Catalyst with Coke Evolution during the Catalytic Pyrolysis of Polyethylene for Fuel Oil. *Appl. Catal., A* **2021**, *609*, 117873.

(21) Dabros, T. M. H.; Stummann, M. Z.; Høj, M.; Jensen, P. A.; Grunwaldt, J. D.; Gabrielsen, J.; Mortensen, P. M.; Jensen, A. D. Transportation Fuels from Biomass Fast Pyrolysis, Catalytic Hydrodeoxygenation, and Catalytic Fast Hydropyrolysis. *Prog. Energy Combust. Sci.* **2018**, *68*, 268−309.

(22) Zheng, N.; Zhang, J.; Wang, J. Parametric Study of Two-Stage Hydropyrolysis of Lignocellulosic Biomass for Production of Gaseous and Light Aromatic Hydrocarbons. *Bioresour. Technol.* **2017**, *244* (July), 142−150.

(23) Santana Junior, J. A.; Menezes, A. L.; Ataíde, C. H. Catalytic Upgrading of Fast Hydropyrolysis Vapors from Industrial Kraft Lignins Using ZSM-5 Zeolite and HY-340 Niobic Acid. *J. Anal. Appl. Pyrolysis* **2019**, *144*, 104720.

(24) Xue, Y.; Sharma, A.; Huo, J.; Qu, W.; Bai, X. Low-Pressure Two-Stage Catalytic Hydropyrolysis of Lignin and Lignin-Derived Phenolic Monomers Using Zeolite-Based Bifunctional Catalysts. *J. Anal. Appl. Pyrolysis* **2020**, *146*, 104779.

(25) Munir, D.; Usman, M. R. Catalytic Hydropyrolysis of a Model Municipal Waste Plastic Mixture over Composite USY/SBA-16 Catalysts. *J. Anal. Appl. Pyrolysis* **2018**, *135* (July), 44−53.

(26) Stummann, M. Z.; Høj, M.; Hansen, A. B.; Davidsen, B.; Wiwel, P.; Gabrielsen, J.; Jensen, P. A.; Jensen, A. D. New Insights into the

Effect of Pressure on Catalytic Hydropyrolysis of Biomass. *Fuel Process. Technol.* **2019**, *193* (May), 392−403.
(27) Hu, Y.; Li, J.; Wang, S.; Xu, L.; Barati, B.; Cao, B.; Wang, H.; Xie, K.; Wang, Q. Catalytic Fast Hydropyrolysis of Seaweed Biomass with Different Zeolite Catalysts to Produce High-Grade Bio-Oil. *Process Saf. Environ. Prot.* **2021**, *146*, 69−76.
(28) Chareonpanich, M.; Boonfueng, T.; Limtrakul, J. Production of Aromatic Hydrocarbons from Mae-Moh Lignite. *Fuel Process. Technol.* **2002**, *79* (2), 171−179.
(29) Melligan, F.; Hayes, M. H. B.; Kwapinski, W.; Leahy, J. J. Hydro-Pyrolysis of Biomass and Online Catalytic Vapor Upgrading with Ni-ZSM-5 and Ni-MCM-41. *Energy Fuels* **2012**, *26* (10), 6080−6090.
(30) He, Y.; Zhao, Y.; Chai, M.; Zhou, Z.; Sarker, M.; Li, C.; Liu, R.; Cai, J.; Liu, X. Comparative Study of Fast Pyrolysis, Hydropyrolysis and Catalytic Hydropyrolysis of Poplar Sawdust and Rice Husk in a Modified Py-GC/MS Microreactor System: Insights into Product Distribution, Quantum Description and Reaction Mechanism. *Renewable Sustainable Energy Rev.* **2020**, *119*, 109604.
(31) Venkatakrishnan, V. K.; Degenstein, J. C.; Smeltz, A. D.; Delgass, W. N.; Agrawal, R.; Ribeiro, F. H. High-Pressure Fast-Pyrolysis, Fast-Hydropyrolysis and Catalytic Hydrodeoxygenation of Cellulose: Production of Liquid Fuel from Biomass. *Green Chem.* **2014**, *16* (2), 792−802.
(32) Chen, W.; Lu, J.; Zhang, C.; Xie, Y.; Wang, Y.; Wang, J.; Zhang, R. Aromatic Hydrocarbons Production and Synergistic Effect of Plastics and Biomass via One-Pot Catalytic Co-Hydropyrolysis on HZSM-5. *J. Anal. Appl. Pyrolysis* **2020**, *147*, 104800.
(33) Chandler, D. S.; Seufitelli, G. V. S.; Resende, F. L. P. Catalytic Route for the Production of Alkanes from Hydropyrolysis of Biomass. *Energy Fuels* **2020**, *34* (10), 12573−12585.
(34) Jan, O.; Marchand, R.; Anjos, L. C. A.; Seufitelli, G. V. S.; Nikolla, E.; Resende, F. L. P. Hydropyrolysis of Lignin Using Pd/HZSM-5. *Energy Fuels* **2015**, *29* (3), 1793−1800.
(35) Gamliel, D. P.; Bollas, G. M.; Valla, J. A. Bifunctional Ni-ZSM-5 Catalysts for the Pyrolysis and Hydropyrolysis of Biomass. *Energy Technol.* **2017**, *5* (1), 172−182.
(36) Chandler, D. S.; Resende, F. L. P. Comparison between Catalytic Fast Pyrolysis and Catalytic Fast Hydropyrolysis for the Production of Liquid Fuels in a Fluidized Bed Reactor. *Energy Fuels* **2019**, *33* (4), 3199−3209.
(37) Venkatakrishnan, V. K.; Delgass, W. N.; Ribeiro, F. H.; Agrawal, R. Oxygen Removal from Intact Biomass to Produce Liquid Fuel Range Hydrocarbons via Fast-Hydropyrolysis and Vapor-Phase Catalytic Hydrodeoxygenation. *Green Chem.* **2015**, *17* (1), 178−183.
(38) Zhang, L.; Gong, K.; Lai, J.; Alvey, P. Chemical Composition and Stability of Renewable Hydrocarbon Products Generated from a Hydropyrolysis Vapor Upgrading Process. *Green Chem.* **2017**, *19* (15), 3628−3641.
(39) Marker, T. L.; Felix, L. G.; Linck, M. B.; Roberts, M. J. Integrated Hydropyrolysis and Hydroconversion (IH2VR) for the Direct Production of Gasoline and Diesel Fuels or Blending Components from Biomass, Part 1: Proof of Principle Testing. *Environ. Prog. Sustainable Energy* **2012**, *31* (2), 191−199.
(40) Marker, T. L.; Felix, L. G.; Linck, M. B.; Roberts, M. J.; Ortiz-Toral, P.; Wangerow, J. Integrated Hydropyrolysis and Hydroconversion (IH2VR) for the Direct Production of Gasoline and Diesel Fuels or Blending Components from Biomass, Part 2: Continuous Testing. *Environ. Prog. Sustainable Energy* **2014**, *33* (3), 762−768.
(41) Gamliel, D. P.; Bollas, G. M.; Valla, J. A. Two-Stage Catalytic Fast Hydropyrolysis of Biomass for the Production of Drop-in Biofuel. *Fuel* **2018**, *216*, 160−170.
(42) Sirous-Rezaei, P.; Park, Y. K. Catalytic Hydropyrolysis of Lignin: Suppression of Coke Formation in Mild Hydrodeoxygenation of Lignin-Derived Phenolics. *Chem. Eng. J.* **2020**, *386*, 121348.
(43) Melligan, F.; Hayes, M. H. B.; Kwapinski, W.; Leahy, J. J. A Study of Hydrogen Pressure during Hydropyrolysis of Miscanthus x Giganteus and Online Catalytic Vapour Upgrading with Ni on ZSM-5. *J. Anal. Appl. Pyrolysis* **2013**, *103*, 369−377.
(44) Gamliel, D. P.; Wilcox, L.; Valla, J. A. The Effects of Catalyst Properties on the Conversion of Biomass via Catalytic Fast Hydropyrolysis. *Energy Fuels* **2017**, *31* (1), 679−687.
(45) Stummann, M. Z.; Høj, M.; Davidsen, B.; Hansen, A. B.; Hansen, L. P.; Wiwel, P.; Schandel, C. B.; Gabrielsen, J.; Jensen, P. A.; Jensen, A. D. Effect of the Catalyst in Fluid Bed Catalytic Hydropyrolysis. *Catal. Today* **2020**, *355*, 96−109.
(46) Stummann, M. Z.; Høj, M.; Schandel, C. B.; Hansen, A. B.; Wiwel, P.; Gabrielsen, J.; Jensen, P. A.; Jensen, A. D. Hydrogen Assisted Catalytic Biomass Pyrolysis. Effect of Temperature and Pressure. *Biomass Bioenergy* **2018**, *115* (May), 97−107.
(47) Dayton, D. C.; Hlebak, J.; Carpenter, J. R.; Wang, K.; Mante, O. D.; Peters, J. E. Biomass Hydropyrolysis in a Fluidized Bed Reactor. *Energy Fuels* **2016**, *30* (6), 4879−4887.
(48) Venkatesan, K.; He, S.; Seshan, K.; Selvam, P.; Vinu, R. Selective Production of Aromatic Hydrocarbons from Lignocellulosic Biomass via Catalytic Fast-Hydropyrolysis Using W_2C/γ-Al_2O_3. *Catal. Commun.* **2018**, *110*, 68−73.
(49) Farinmade, A.; Ajumobi, O.; Yu, L.; Su, Y.; He, J.; Valla, J. A.; John, V. A One-Step Facile Encapsulation of Zeolite Microcrystallites in Ordered Mesoporous Microspheres. *Ind. Eng. Chem. Res.* **2020**, *59* (31), 13923−13931.
(50) Du, S.; Sun, Y.; Gamliel, D. P.; Valla, J. A.; Bollas, G. M. Catalytic Pyrolysis of Miscanthus × giganteus in a Spouted Bed Reactor. *Bioresour. Technol.* **2014**, *169*, 188−197.
(51) Maia, A. J.; Louis, B.; Lam, Y. L.; Pereira, M. M. Ni-ZSM-5 Catalysts: Detailed Characterization of Metal Sites for Proper Catalyst Design. *J. Catal.* **2010**, *269* (1), 103−109.
(52) Kruk, M.; Jaroniec, M.; Sakamoto, Y.; Terasaki, O.; Ryoo, R.; Ko, C. H. Determination of Pore Size and Pore Wall Structure of MCM-41 by Using Nitrogen Adsorption, Transmission Electron Microscopy, and X-Ray Diffraction. *J. Phys. Chem. B* **2000**, *104* (2), 292−301.
(53) Takenaka, S.; Shimizu, T.; Otsuka, K. Complete Removal of Carbon Monoxide in Hydrogen-Rich Gas Stream through Methanation over Supported Metal Catalysts. *Int. J. Hydrogen Energy* **2004**, *29* (10), 1065−1073.
(54) Zhang, H.; Shao, S.; Luo, M.; Xiao, R. The Comparison of Chemical Liquid Deposition and Acid Dealumination Modified ZSM-5 for Catalytic Pyrolysis of Pinewood Using Pyrolysis-Gas Chromatography/Mass Spectrometry. *Bioresour. Technol.* **2017**, *244* (June), 726−732.
(55) Muroyama, H.; Tsuda, Y.; Asakoshi, T.; Masitah, H.; Okanishi, T.; Matsui, T.; Eguchi, K. Carbon Dioxide Methanation over Ni Catalysts Supported on Various Metal Oxides. *J. Catal.* **2016**, *343*, 178−184.
(56) Yan, X.; Liu, Y.; Zhao, B.; Wang, Z.; Wang, Y.; Liu, C. J. Methanation over Ni/SiO_2: Effect of the Catalyst Preparation Methodologies. *Int. J. Hydrogen Energy* **2013**, *38* (5), 2283−2291.
(57) Mimmo, T.; Panzacchi, P.; Baratieri, M.; Davies, C. A.; Tonon, G. Effect of Pyrolysis Temperature on Miscanthus (Miscanthus × Giganteus) Biochar Physical, Chemical and Functional Properties. *Biomass Bioenergy* **2014**, *62* (0), 149−157.

https://doi.org/10.1021/acs.energyfuels.1c02453
Energy Fuels 2021, 35, 20117−20130